Point-Bonded Polymer Nonwovens and Their Rupture in Stretching

Wenshuo Zhang[1], Christopher Staszel[1], Alexander L. Yarin[1*], Eunkyoung Shim[2], Behnam Pourdeyhimi[2]

[1]Department of Mechanical and Industrial Engineering,
University of Illinois at Chicago,
842 W. Taylor St., Chicago, IL 60607-7022, United States

[2]3427 The Nonwovens Institute, Box 8301,
North Carolina State University
Raleigh, NC 27695-8301, United States

Abstract

The work aims at the experimental investigation and theoretical modeling of the physical phenomena responsible for thermal bonding of polymer fibers in nonwovens and their effect on such mechanical properties as the nonwoven stiffness, the yield stress, the stress at failure, toughness, and the entire stress-strain curve. In the experiments two types of nonwovens were explored: Polybutylene Terephthalate (PBT) nonwoven and
* Correspondence should be addressed to E-mail: ayarin@uic.edu. Phone: +1(312) 996-3472. Fax: +1(312) 413-0447.

.

Polybutylene Terephthalate (PBT)/Polyethylene (PE) (80/20) nonwoven. Special attention was paid to the effect of the bonding pattern (e.g. circular or rhombic) on the nonwoven failure patterns in stretching. It was shown that failure happens at the periphery of stiffened bonds. A theory of this phenomenon is given which predicted tensile stress concentration up to 140% of the applied tensile stress in that area, which was responsible for the failure modes observed experimentally.

1. Introduction

The inter-fiber bonding area and/or bonding patterns in nonwovens fully determine such properties as the machine direction (MD) and cross-direction (CD) tensile stiffness (Young's modulus), elasticity, softness, compressibility, absorptivity, etc. These properties are determined by such factors as melt temperature and the degree of crystallinity and solidification when nonwovens are formed by meltblowing. When nonwovens are formed by solution blowing, the degree of solvent evaporation and fiber dryness and the degree of crystallinity dictate the final strength. In both cases of melt- and solution blowing of nonwovens, further strength is achievable by means of point-bonding, namely the thermal compression of bond area patterns across the nonwovens. Such bonding is driven by sintering and adhesion of the polymer fibers at the bond region, significantly increasing the physical strength of the nonwoven web.

The adhesion is the physical process of joining separate surfaces of materials (or fibers in a nonwoven [1]) together through mechanical, chemical, or thermodynamic bonding. In the present case of thermal point-bonding of nonwovens, the polymers typically do not react and the adhesion and strength at such a bond point is driven by the

diffusion and entanglement of polymer chains through the surfaces in contact [1-5]. This diffusion process is due to the thermodynamically-driven reptation of polymer chains, resulting in their entanglement and formation of the adhesive strength at the interface [2, 5-7]. In several important experiments such as [3, 4], it was observed that the diffusion of polymer chains is a two-step process. Initially, polymer chains quickly diffuse across the surfaces in contact, interlocking and leaving what are referred to as “runners”, or un-entangled sections of the polymers, at the surface [3, 4]. At this initial stage, most of the adhesive energy is gained and afterwards the system slowly relaxes toward an equilibrium with all ‘runners’ completely diffusing across the interface [3, 4]. A notable theoretical work on the dynamics of the diffusion stages has been conducted in [8, 9].

Such understanding of the polymer diffusion and entanglement is already used industrially in the creation of point-bonded nonwoven webs [1]. Accordingly, experiments with bonds of various contacting areas were conducted and discussed in [10]. It is understood that processing times and point-bonding times should be chosen to allow melting of the crystalline regions in the nonwoven as well as a sufficient time for reptation and entanglement of interfused polymer chains across the fibers. The effect of thermal bonding on the microscopic level is akin to annealing at high temperature, past the glass transition temperature, and is used to enhance mechanical performance at the bond sight. Various works have demonstrated such a phenomenon associated with thermal bonding of nonwovens as an increase in the crystal sizes [10]. In addition, the explanation of the crystallization behavior of PE and PBT, as well as the crystallized polymer structure and the degree of crystallinity is available in [11-16]. The changes in

the degree of crystallinity of several other polymer caused by thermal bonding are available in [17].

Furthermore, it is understood that pressure due to point-bonding can increase the melting point of polymers due to the Clapeyron effect [1, 18]. Thermal degradation at the bond point has also been researched, leading to the conclusion that high bonding temperatures or long bonding times will result in deterioration of modulus of elasticity at the bond points [19-21]. A further decrease in Young's modulus in a point-bonded nonwoven web can also be explained by the issues related to poor polymer compatibility. Adhesion between polymers is related to their miscibility, or often immiscibility of polymers brought in contact. The adhesion between dissimilar polymers is typically weak [2, 7]. To address these limitations, bi-component fibers have been employed with the main aim of enhancing the mechanical strength of fibrous composite materials [19, 21].

In the existing works, such processing conditions as temperature, bond pressure, and polymer micro-mechanics (reptations) and various other aspects of the point-bonding process have been addressed. However, the failure patterns at the bond periphery and their reasons remain mostly unexplored. In a point-bonded nonwoven, high-stiffness (point-bonded) domains are imposed in an elastic material of lower stiffness (the nonwoven web) as a means of increasing the overall mechanical properties. In this situation, it is of significant interest to understand whether such a stiff inclusion can act as a stress concentrator in the nonwoven web and lead to a premature failure due to over-bonding. An insight in these phenomena is of significant importance.

Elastic problems related to stretching of material with an inclusion (understood in the present work as a thermal bond) stem from the seminal work of Kirsch [22], who solved

the planar problem on uniaxial stretching of an elastic material with a circular hole. The important developments motivated by mechanics of composite materials can be found in [23, 24], which are the works which dealt with elastic inclusions. A more recent interest to the problem is related to materials with nano-inclusions, where the stress field in an isotropic plane under uniaxial stretching with a circular inclusion was calculated in [25]. The approach of the latter work does not imply the complex elastic potentials, which significantly simplify calculations.

The present work aims at further understanding the effect of thermal point-bonding inclusions on nonwoven webs as a means of increasing mechanical performance. Here, experiments are conducted to understand the effect of point bonding in nonwovens on the mechanical performance as well as on failure patterns. A theory is also given using the complex elastic potentials (i.e. the Goursat functions) in the framework of the general approach of the planar problem of the theory of elasticity dating back to Kolosov and Muskhelishvili [26-28].

2. Experimental

2.1 Materials

Two meltblown nonwoven mats were chosen for this work, Polybutylene Terephthalate (PBT) (which will be designated as PBT nonwoven) as well as a nonwoven composed of a mixture of 80 % Polybutylene Terephthalate and 20 % Polyethylene (PE) (which will be designated as PBT/ PE 80/20 nonwoven). The PBT nonwoven had the basis weight of 100 GSM (gram per square) with the average measured thickness of 0.33 mm. The PBT/PE 80/20 nonwoven had the basis weight of 75 GSM with the average

measured thickness of 0.30 mm. The nonwovens tested were all cut into 15 mm × 90 mm rectangular samples from the nonwoven sheets in the same direction.

In the present work, the as received nonwovens were pre-bonded using a standard point-bonding process. As will be discussed in the following section, further bonding was conducted by significantly larger circular and rhombic punches at the center of these nonwoven strips to understand the effect of bonding and the corresponding rupture pattern. Such an additional bond would be significantly stronger then the surrounding bonds as corroborated by the rupture patterns elucidated by the following results. Thus, it can be assumed that the minor pre-bonding had a minimal effect compared to the further bonding process used in this work.

2.2 Thermal bonding

In the present work the nonwovens were further thermally bonded using the setup depicted in Fig. 1a.

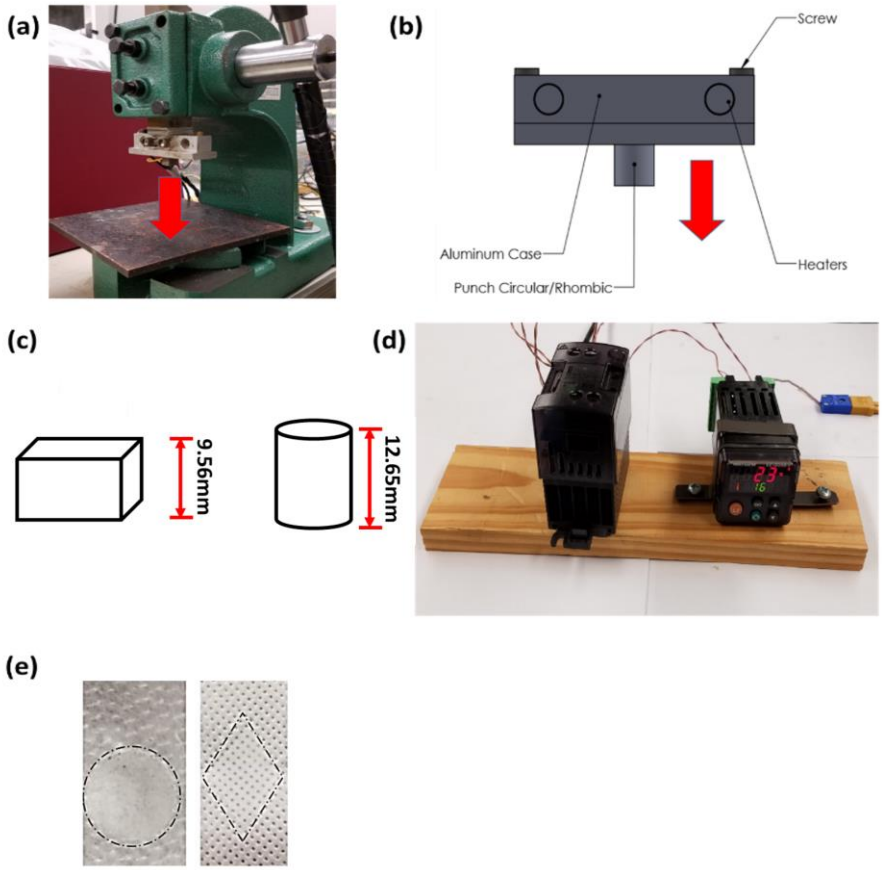

Fig. 1. (a) Thermal bonding setup for the additional bond patterning with the aluminum case attached and used for point bonding. (b) Schematic of the aluminum case with an interchangeable thermal punch inserted. (c) Schematic of two types of thermal punches, rhombic and circular. (d) The temperature controller (Watlow EZ-ZONE). (e) Example of PBT nonwoven sample with a single circular bond pattern as well as a single rhombic bond pattern formed by the setup of panel (a).

The main part of the setup was an Arbor press used to advance and compress a nonwoven using an aluminum case containing interchangeable heated punches (either circular or rhombic in cross-section) (cf. Fig. 1a and 1b). The diameter of the circular

punch was 12.60 mm and its surface area was 124.59 mm^2, whereas the rhombic punch had a length of 18.90 mm, width of 12.65 mm, and the total surface area of 119.54 mm^2 (cf. Fig. 1c). The aluminum case and the interchangeable punch were heated using an embedded cartridge heater (CSH- 201200/120V). A thermocouple (Omega model 5TC-PVC-T-24-180) was embedded in the various interchangeable punches. A temperature controller (Watlow EZ-ZONE) (cf. Fig. 1d) was also included. Using such a configuration, the temperature of the front face of the interchangeable punches was regulated to various constant set temperatures for thermal bonding.

The heated interchangeable punch (either circular or rhombic) was advanced and contacted the central portion of the rectangular nonwoven samples and formed additional thermal bonding patterns on them. The contact time of the punch with the samples was maintained as 1 s. For the case of the PBT nonwovens, thermal bonding was conducted at constant temperature of 190 °C, whereas for the case of the PBT/ PE 80/20 nonwovens, the constant temperatures chosen were 110 °C as well as 120 °C. These temperatures were chosen to ensure full thermal bonding (the melting point of PBT is 220 °C [29] and of PE is 110-126 ºC [29]). An example of a PBT nonwoven bonded with either circular or rhombic punch is shown in Fig. 1e.

2.3 Tensile tests of bonded nonwovens

Tensile tests of the original and the additionally bonded samples were conducted using an Instron machine (model 5942) with a 100 N load cell to obtain the entire stress-strain curves of the as-received original PBT nonwovens and the PBT/PE 80/20 nonwovens, as well as those nonwoven samples which underwent thermal bonding as

described in sub-section 2.2. The samples were clamped firmly in place by pneumatic clamps with an initial test length of 40 mm and advanced at a rate of 2 mm/min. For each type of samples tested, 10 tensile trials were conducted.

The Young's modulus and yield stress were determined from the acquired data using the following phenomenological Green's equation fitted to the acquired stress-strain curves [30, 31]

$$\sigma_{yy} = Y \tanh\left(\frac{E}{Y}\varepsilon_{yy}\right) \quad (1)$$

Here σ_{yy} is the tensile stress, ε_{yy} the tensile strain (with y being the stretching direction), E is Young's modulus, and Y - the yield stress. This equation implies perfect plasticity and was fitted to the experimental data so that the elastic region was approximated first with a minimum coefficient of determination R^2 of at least 0.999.

The toughness T of the nonwoven samples, i.e. the specific energy associated with tensile deformation was found using the following equation

$$T = \int \sigma_{yy} d\varepsilon_{yy} \quad (2)$$

2.4 Imaging

Images of nonwovens were taken by a DSLR camera with setting of f= 3.5 and 1/60 exposition time. All images were taken under the same conditions.

3. Results and Discussion

3.1 Results of the tensile tests of the as-received nonwovens as well as the bonded nonwovens

Tensile tests were conducted using the as-received PBT nonwovens and PBT/ PE 80/20 nonwovens. Several examples of the stress-strain curves for these nonwovens are shown in Figs. 2-4.

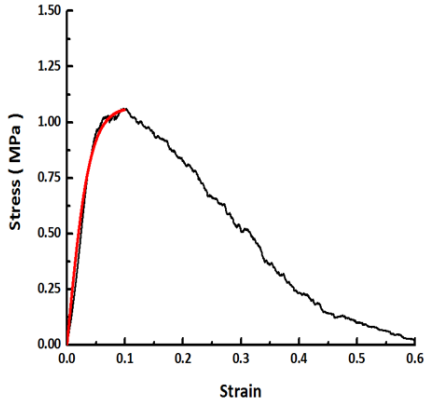

Fig. 2. An example of the stress-strain curve of the as-received PBT nonwovens measured in tensile tests. The data is shown by the black curve, the phenomenological Green equation (1) fit- by the red curve.

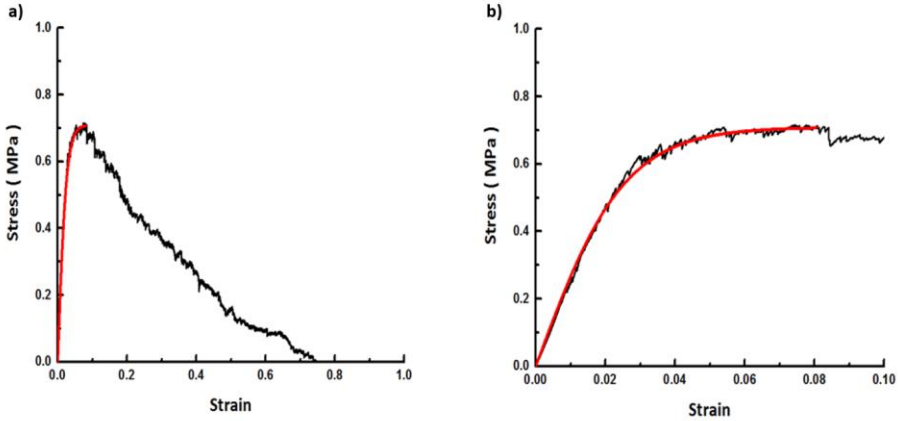

Fig. 3. (a) An example stress-strain curve of the as-received PBT/ PE 80/20 nonwovens measured in tensile tests. The data is shown by the black curve, the phenomenological Green equation (1) fit- by the red curve. (b) A zoomed-in view of the elastic section followed by the perfectly plastic section.

From the results obtained in the tensile tests, the average Young's modulus E and the yield stress Y revealed by the phenomenological Eq. (1) were found. Also, the toughness T revealed by Eq. (2) for both the as-received PBT nonwoven as well as the as-received PBT/PE 80/20 nonwoven was determined. In addition, the maximum stress at failure σ_{max} was found. These results are presented in Table 1 and depicted in Fig. 4.

Table 1. Average mechanical properties of the as-received PBT and PBT/PE 80/20 nonwovens.

Nonwoven type	Average Young`s modulus E (MPa)	Average yield stress Y (MPa)	Average toughness T (MPa)	Average maximum stress at failure σ_{max} (MPa)
As- received PBT	34.521 ± 6.133	1.169 ± 0.104	0.320 ± 0.066	1.167 ± 0.098
As- received PBT/PE 80/20	27.397 ± 10.520	0.646 ± 0.137	0.410 ± 0.090	0.628 ± 0.119

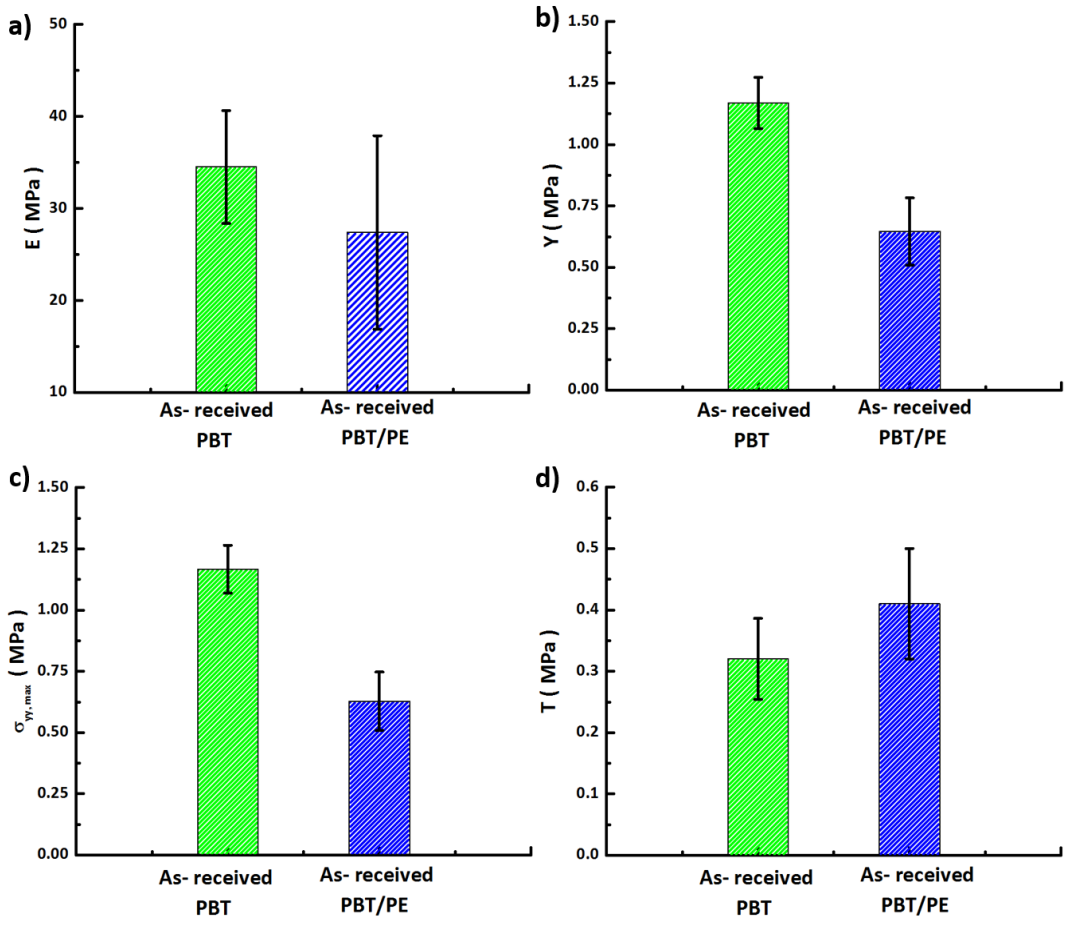

Fig. 4. Mechanical properties in tension of the as-received PBT and PBT/PE 80/20 nonwovens. (a) Average values of Young's modulus E. (b) Average values of the yield stress Y. (c) Average values of the maximum stress ($\sigma_{yy,\,max}$). (d) Average values of the toughness (T).

As seen in Table 1 and Fig. 4, the as-received PBT nonwovens revealed a higher Young's modulus E, the yield stress Y, and the maximum stress σ_{max} than those of the PBT/ PE 80/20 nonwovens. On the other hand, the toughness (T) of the as-received PBT/ PE 80/20 nonwovens was higher than that of the as-received PBT nonwovens, which is

related to a prolonged plastic deformation of the former prior to the failure. Furthermore, the as-received PBT/ PE 80/20 nonwovens also revealed a section of a perfectly plastic behavior at which the tensile stress practically plateaus and Green's equation approximates the data very accurately (Fig. 3b).

3.2 Results of the tensile tests of the thermally bonded nonwovens

Tensile tests were conducted with PBT nonwovens and PBT/ PE 80/20 nonwoven samples modified by a single circular thermal bond as well as by a single rhombic thermal bond. For the case of the PBT nonwoven, thermal bonding was conducted at a temperature of 190 °C, as for the PBT/ PE 80/20 nonwovens the bonding temperatures chosen were 110 °C as well as 120 °C. Several examples of stress-strain curves for these nonwovens bonded with a circular and rhombic bond are shown in Figs. 5 and 6.

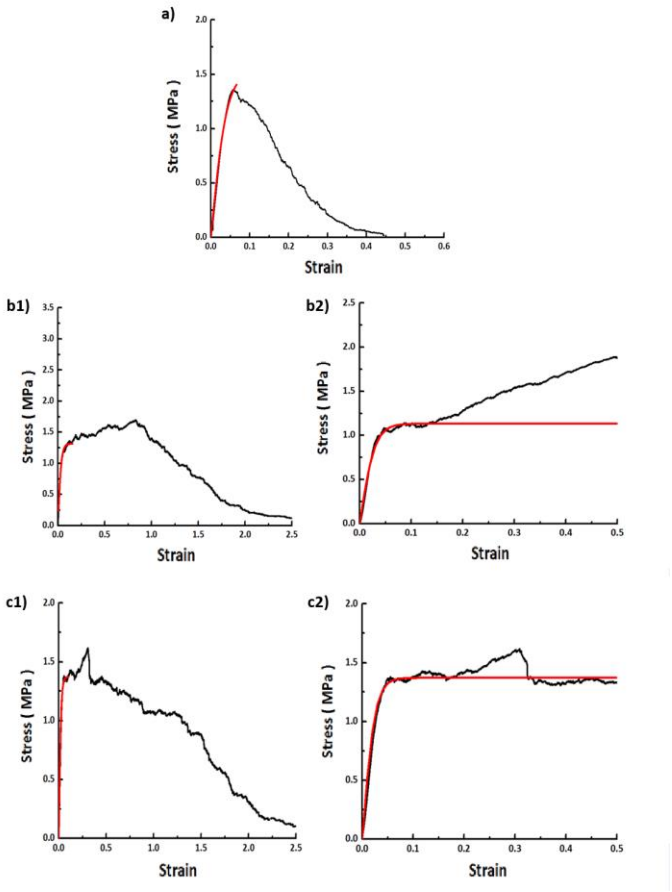

Fig. 5. Examples of the stress-strain curves of the nonwoven samples bonded with an additional single circular bond. (a) The PBT nonwoven bonded by a circular bond at 190 °C. (b1) The PBT/ PE 80/20 nonwoven bonded by a circular bond at 120 °C and (b2) a zoomed-in view of the elastic region. (c1) The PBT/ PE 80/20 nonwoven bonded by a circular bond at 110 °C and (c2) a zoomed-in view of the elastic region. The data is shown by the black curves, the Green equation fit- by the red curves.

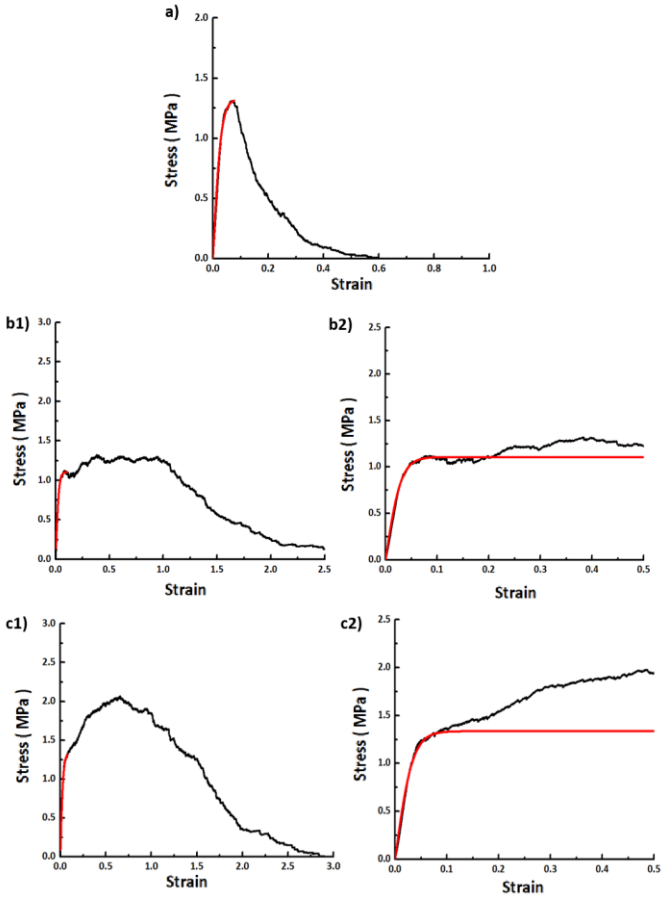

Fig. 6. Examples of the stress-strain curves of the nonwoven samples bonded with an additional single rhombic bond. (a) The PBT nonwoven bonded by a rhombic bond at 190 °C. (b1) The PBT-PE nonwoven bonded by a rhombic bond at 120 °C and (b2) a zoomed-in view of the elastic region. (c1) The PBT/ PE 80/20 nonwoven bonded by a rhombic bond at 110 °C and (c2) a zoomed-in view of the elastic region. The data is shown by the black curves, the Green equation fit- by the red curves.

From the stress-strain curves obtained for the PBT nonwovens as well as the PBT/PE 80/20 nonwovens, both thermally bonded with the circular punch as well as the rhombic punch, the average Young's modulus E, the yield stress Y, toughness T, and the

maximum stress at failure σ_{max} were determined. These results are presented in Table 2. In Figs. 7 and 8, the results for these mechanical properties for the as-received nonwovens are compared to those of the thermally bonded nonwovens.

Table 2. Average mechanical properties of bonded PBT and PBT/PE 80/20 nonwovens.

Nonwoven name	Average Young`s modulus E (MPa)	Average yield stress Y (MPa)	Average toughness T (MPa)	Average maximum stress at failure σ_{max} (MPa)
Circular bonded PBT	36.847 ± 4.699	1.455 ± 0.288	0.289 ± 0.052	1.364 ± 0.230
Rhombic bonded PBT	41.200 ± 5.652	1.355 ± 0.288	0.254 ± 0.040	1.310 ± 0.202
110 ºC Circular bonded PBT/ PE 80/20	36.057 ± 10.346	1.117 ± 0.194	2.222 ± 0.395	1.127 ± 0.193
110 ºC Rhombic bonded PBT/ PE 80/20	41.657 ± 7.787	1.209 ± 0.240	2.527 ± 0.638	1.198 ± 0.263
120 ºC Circular bonded PBT/ PE 80/20	37.856 ± 7.382	1.273 ± 0.216	2.477 ± 0.890	1.260 ± 0.215
120 ºC Rhombic bonded PBT/ PE 80/20	40.932 ± 5.401	1.241 ± 0.224	2.410 ± 0.626	1.226 ± 0.197

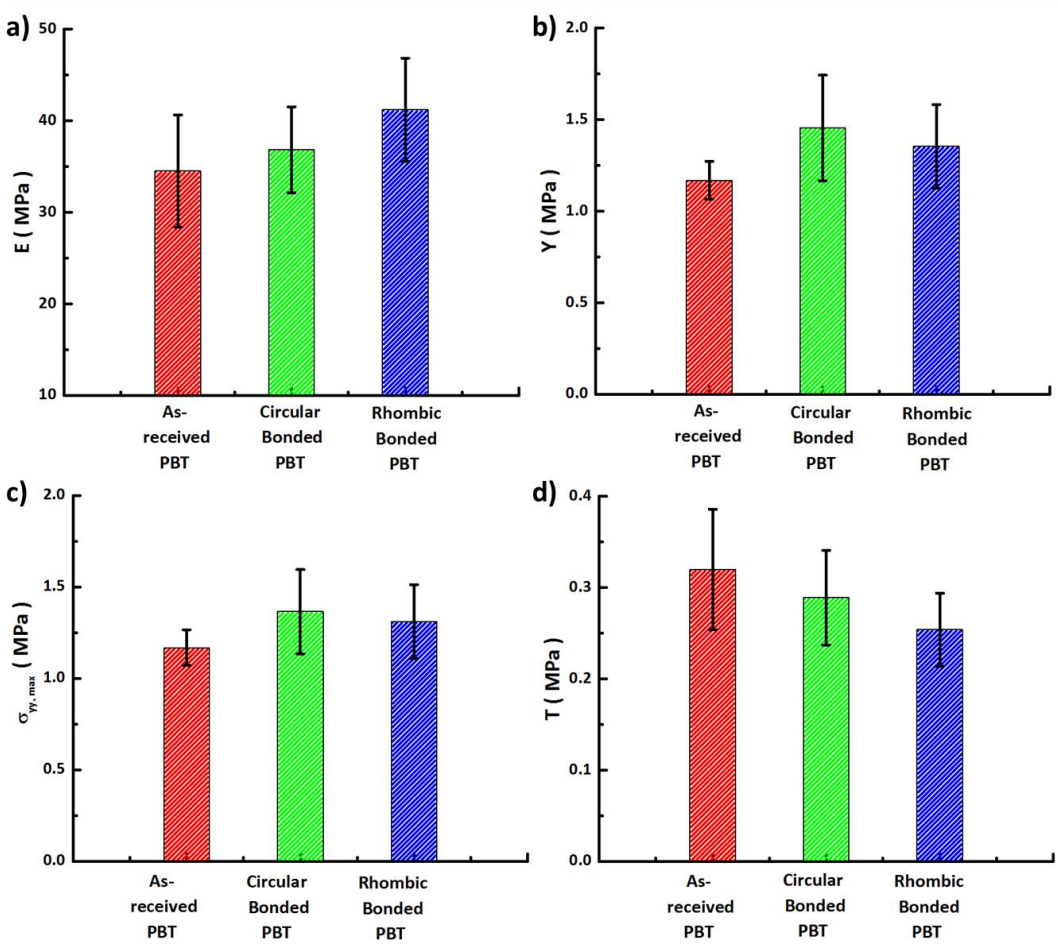

Fig. 7. Mechanical properties of the as-received PBT nonwovens, PBT nonwovens with an additional single circular bond imposed at 190 ºC, and PBT nonwovens with an additional single rhombic bond imposed at 190 ºC. (a) Average values of Young`s modulus. (b) Average values of the yield stress. (c) Average values of the maximum stress at failure. (d) Average values of toughness.

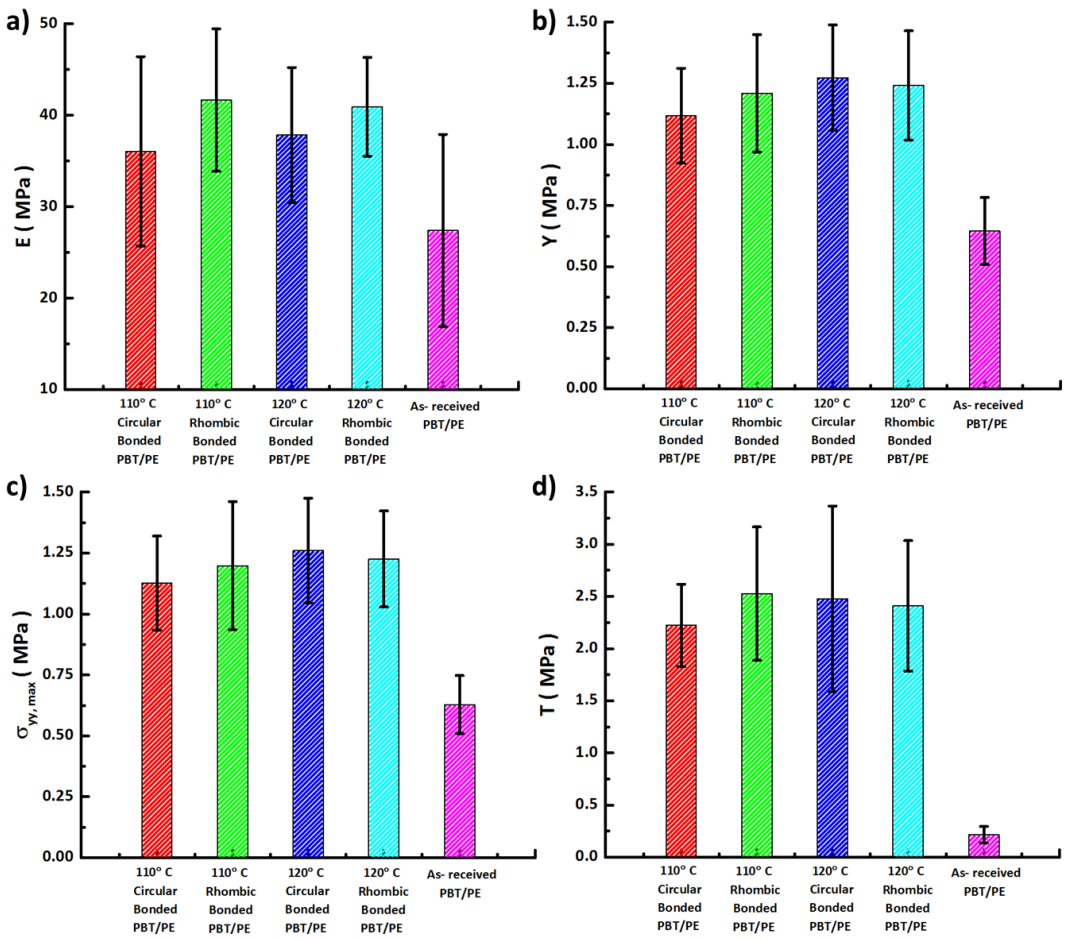

Fig. 8. Mechanical properties of the as-received PBT/PE 80/20 nonwovens in comparison with those bonded at 110 ºC and 120 ºC with a single circular or rhombic bond. (a) Average values of Young`s modulus. (b) Average values of the yield stress. c) Average values of the maximum stress. (d) Average values of toughness.

From the results presented in Figs. 7 and 8, various conclusions on the effect of bonding can be made. For the case of both PBT nonwovens as well as PBT/PE 80/20 nonwovens, an additional circular or rhombic bond will increase Young's modulus, the yield strength, and the maximum stress as compared to the as-received nonwovens.

However, in the case of the PBT nonwovens, the additional bonds decreased the toughness.

Such a decrease in the toughness of the PBT nonwoven samples can be explained by the fact that a thermal bond acts as a stress concentrator inside the nonwoven sample. As will be corroborated by the theoretical stress fields in sub-section 3.4, the increased stresses at the bond periphery are observed when an inclusion of a higher stiffness (the thermal bond) is added to the nonwoven. Due to such inclusions, the nonwoven stiffness increased overall. However, the bonds acted as stress concentrators and led to an earlier failure and as a result, a decrease in toughness. Furthermore, comparing the toughness of the PBT nonwoven with a circular bond to that with a rhombic bond, the increased stresses at the bond periphery of the rhombic shape compared to the circular one also led to a further decrease in the toughness. Such phenomena will be further discussed in the following sub-section 3.3.

For the case of the PBT/PE 80/20 nonwoven, a decrease in toughness was not observed. In this nonwoven, bonding was conducted to only melting point of PE which bonded the web of PBT. Such a bonding allowed for the high stresses at the bond periphery to be alleviated in the PBT/ PE 80/20 nonwoven. This alleviation in the rupture in the nonwoven was likely caused by the breaking of the PBT/PE 80/20 bond and a slowed failure leading to an increase in the overall toughness of the nonwoven.

The overall increase in the yield stress, and the maximum stress as well as the decrease in Young's modulus in the case of the circular punch, as opposed to the rhombic punch, is likely a manifestation of the fact that the area of the circular bond is slightly larger than that of the rhombic bond (the area of the circular bond is 124.59 mm^2 and that

of the rhombic one is 119.54 mm^2). Accordingly, comparing the results for these two types of bonds, one can conclude that a larger bonding area facilitates an increase in the yield stress and the maximum stress values before failure, albeit decreases Young`s modulus.

Comparing bonding the PBT/ PE 80/20 nonwovens at 110 °C to that at 120 °C for either circular bonds or rhombic bonds, one is tempted to conclude that the higher bonding temperature results in a minimal overall increase in the mechanical properties. However, due to the large standard deviation in the results obtained, no clear conclusion can be made.

3.3 Rupture patterns

The rupture patterns at the bond periphery in the bonded nonwovens can be clearly seen after tensile tests. The as-received PBT nonwoven before and after testing as well as those with the circular- and rhombic-shaped bonds are shown in Fig. 9. The as-received PBT/ PE 80/20 nonwovens before and after tensile tests as well as those with the circular- and rhombic-shaped bonds at 110 °C and 120 °C are shown in Fig. 10. Only a single sample of rupture of each nonwoven is shown here for the sake of brevity.

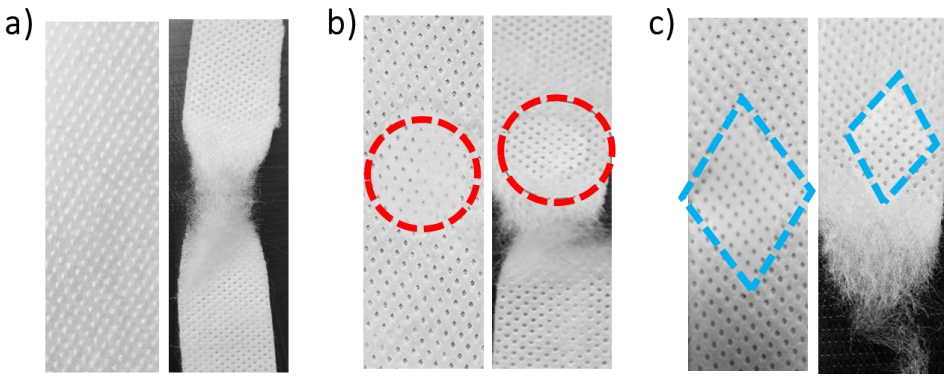

Fig. 9. Examples of the effect of stretching in tensile tests on rupture patterns. (a) The as-received PBT nonwoven before and after tensile test, (b) the PBT nonwoven with a circular bond before and after tensile test, and (c) the PBT nonwoven with a rhombic bond before and after tensile test. The red and blue dashed lines encompass the bond pattern implemented on the circular bonded as well as rhombic bonded samples.

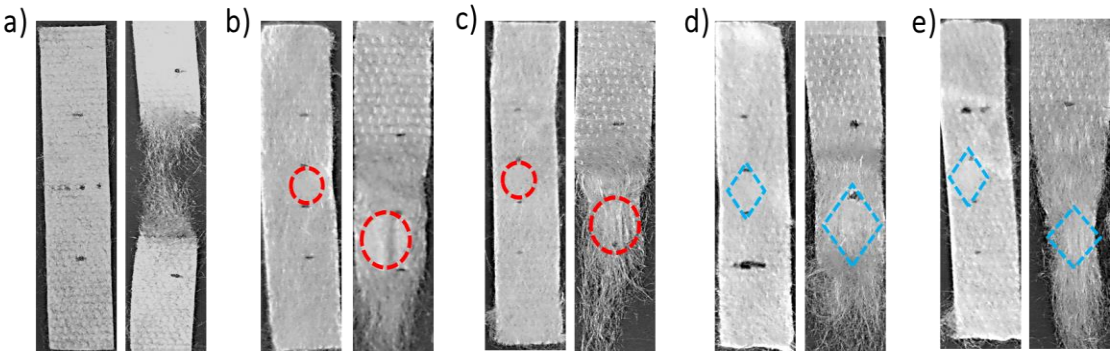

Fig. 10. Examples of the effect of tensile test on rupture patterns. (a) The as-received PBT/PE 80/20 nonwoven before and after tensile test, (b) the PBT/PE 80/20 nonwoven with a 110 °C circular bond before and after tensile test, (c) the PBT/PE 80/20 nonwoven with a 120 °C circular bond before and after tensile test, (d) the PBT/PE 80/20 nonwoven with a 110 °C rhombic bond before and after tensile test, and (e) the PBT/PE 80/20 nonwoven with a 120 °C rhombic bond before and after tensile test. The red and blue dashed lines encompass the bond pattern implemented on the circular bonded as well as rhombic bonded samples. Black dots and horizontal lines on the samples were drawn to facilitate the experiments and do not represent holes.

From the failure patterns depicted in Figs. 9 and 10, it is seen that rupture in the as-received nonwoven samples occurred at the center due to the elongation in tensile tests.

However, for the bonded samples, the rupture happens around the bond periphery (see Figs. 9b-c and 10b-e). Note that such rupture patterns around the periphery were observed in all 10 samples in the tests conducted for the circular punches as well as the rhombic punches in the PBT-nonwoven and also the PBT/PE 80/20 nonwoven. Such a result further corroborates the results related to sample toughness discussed in sub-section 3.2. There it was observed that failure at the bond periphery was due to the stress concentration caused by the bonds. Furthermore, this phenomenon leads to a decrease in toughness of the PBT nonwovens.

3.4 Theoretical prediction of the stress concentration and rupture location

The theoretical solutions of the problem on the stress distributions surrounding a circular thermal bond obtained in Appendix and providing insights into the experimentally observed failure patterns are illustrated below. As an example, the parameter values used were: The ratio of the Young's moduli of the bond and the surrounding matrix $E_2/E_1=10$, the Poisson's ratios of the bond and the surrounding matrix $\nu_1=1/2$, $\nu_2=0.4$, respectively, and the ratio of the stretching stress to Young's modulus of the matrix $\sigma/E_1=0.1$. In all the figures below the coordinates and displacements are rendered dimensionless by the radius of the inclusion circle (the bond) R, and the stresses-by the stretching stress σ.

Fig. 11 shows the field of v and Fig. 12 shows the field of u in material 1 plotted using Eqs. (A19)-(A21), (A26) and (A27) from the Appendix.

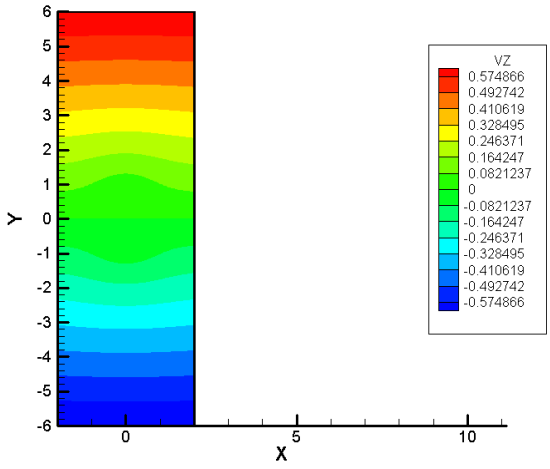

Fig. 11. The field of displacement in the direction of stretching y.

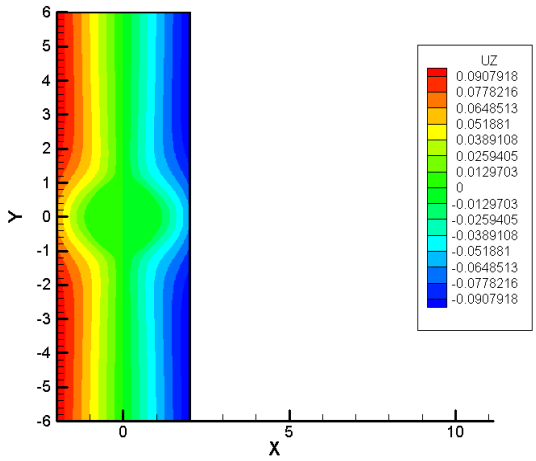

Fig. 12. The field of displacement in the x direction, i.e. normal to the direction of stretching.

Fig. 13 shows the displacement in the direction of stretching in the outer material along the direction of stretching y plotted using Eq. (A29) from the Appendix

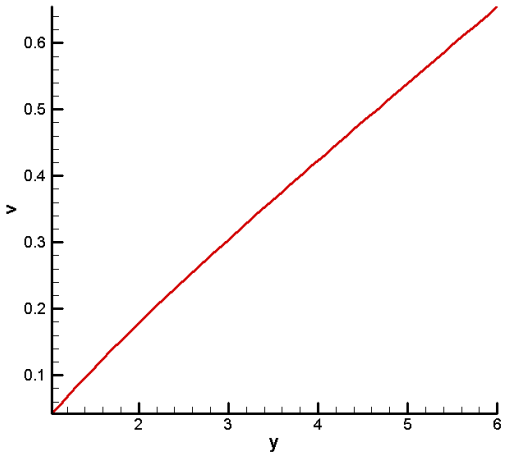

Fig. 13. Displacement in material 1 along the stretching axis.

The stress fields in the entire material 1 and the inclusion 2 plotted using Eqs. (A31)-(A41) from the Appendix are shown in Figs. 14-16.

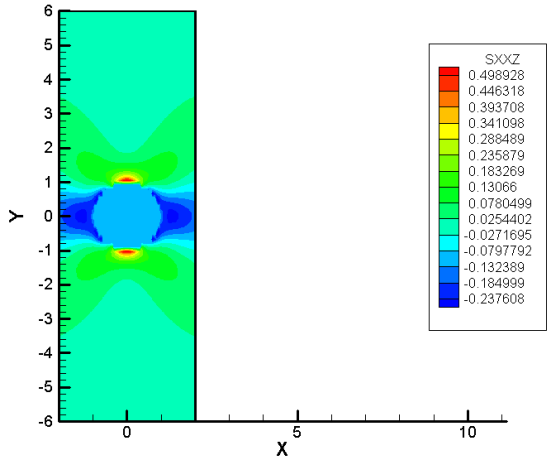

Fig. 14. The stress field σ_{xx}.

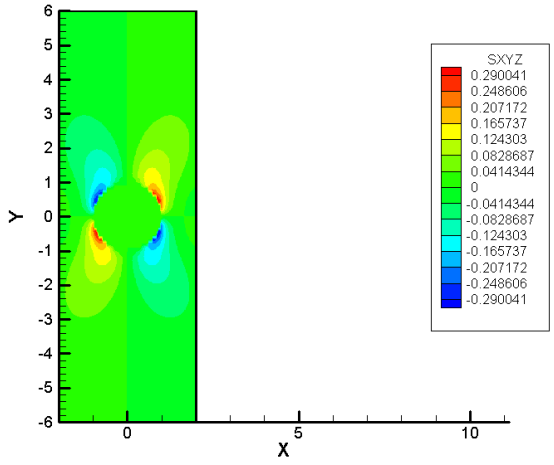

Fig. 15. The stress field σ_{xy}.

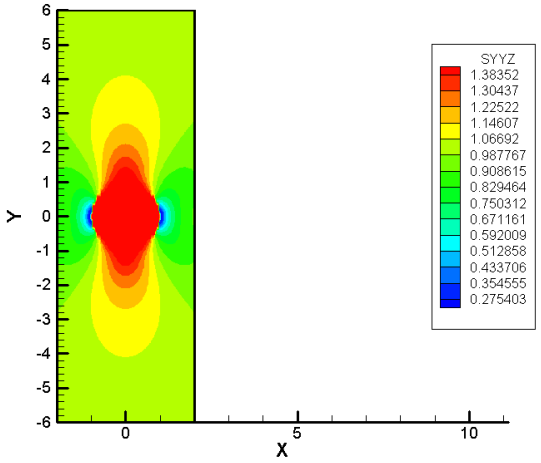

Fig. 16. The stress field σ_{yy}.

The stretching stress σ_{yy} near the inclusion in Fig. 16 exceeds the stretching stress at infinity by about 40%. These results show that a thermal bond acts as a stress concentrator, which triggers rupture at its periphery. Comparing this prediction to the experimental results, it is implied that such a stress concentration led to an early failure of a bonded PBT nonwoven and as a result, decrease in its toughness. Moreover, the failure

patterns at the bond peripheries in Figs. 9 and 10 are also in a qualitative agreement with this prediction.

It should be emphasized that a dramatic increase in the crystallinity of the bond point and the corresponding increase in the value of E_2 would likely lead to a further increase in stress at the bond point periphery during stretching. Such an increase in the stress would lead to an early rupture at the periphery, as the results of the tensile tests and the theory demonstrate. This prediction also agrees with the work [1] where it was demonstrated that there exists an optimum bonding temperature corresponding to a desirable increase in the mechanical strength of nonwovens is reached.

4. Conclusion

The experimental investigation in tensile tests of the effect of the additional thermal bonds on two types of nonwovens, PBT nonwoven and PBT/PE 80/20 nonwoven, elucidated the effect of thermal bonding on the overall mechanical performance. It was found that the addition of a bond, either circular or rhombic, increased the nonwoven stiffness, the yield strength, and the maximum stiffness for both types of nonwovens tested. However, when a PBT nonwoven was bonded, a decrease in toughness was observed. Such a decrease was due to an increased stress at the bond periphery (the stress concentration there) facilitating failure. A theory was also presented which demonstrated that thermal bonds act as stress concentrators, increasing the tensile stress up to 140% at the bond periphery. Such an increase in tensile stress can and does trigger failure at the bond periphery as revealed by the failure patterns experimentally.

In the PBT/PE 80/20 nonwovens, a further increase in the toughness of the nonwoven samples was apparent, which was significantly different from the phenomena observed in the PBT nonwovens. This occurred because during bonding of PBT/PE 80/20 nonwovens, only PE fibers melted and bonded the un-melted PBT fibers, interlocking the web. Due to such interlocking, these bonds would compensate for the increased stress at the bond periphery. Here, these bonds would most likely slowly rupture during tensile tests and as a result, lead to an overall increase in the toughness of such a material.

Due to larger bonding area of the circular bond in comparison to that of the rhombic bond, an increase in the yield stress and the maximum stress at failure was observed in the former case. Such an increased area can also explain a lower Young's modulus resulting from the rhombic bonding.

ACKNOWLEDGEMENT

This work is supported by the Nonwovens Institute, grant No. 16-196.

Appendix: The origin of the rupture pattern surrounding bonds

The origin of the failure patterns surrounding the additional thermal bonds can be traced to the classical Kirsch problem and its extension discussed in the present section. The Kirsch problem describing stretching of an elastic medium with a circular hole of radius R along the y-axis by stress $\sigma_{yy}=\sigma$ at infinity is sketched in Fig. A1.

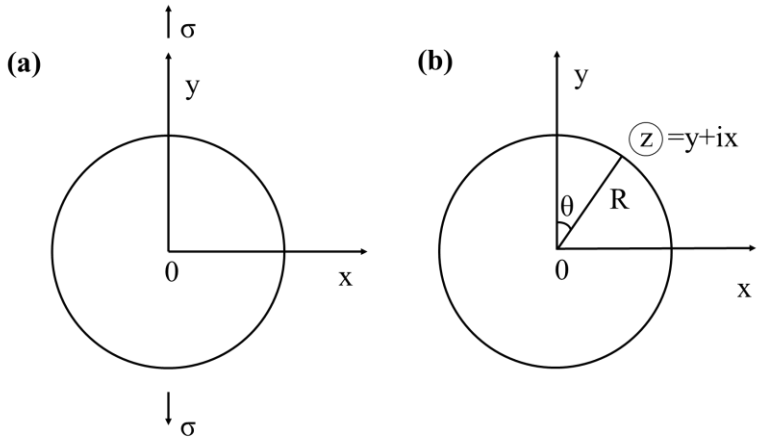

Fig. A1. (a) Sketch of the Kirsch problem. (b) The polar coordinates and the complex z-plane.

The corresponding stress field reads

$$\sigma_{rr} = \frac{\sigma}{2}\left(1-\frac{R^2}{r^2}\right)+\frac{\sigma}{2}\left(1+\frac{3R^4}{r^4}-\frac{4R^2}{r^2}\right)\cos 2\theta \tag{A1}$$

$$\sigma_{\theta\theta} = \frac{\sigma}{2}\left(1+\frac{R^2}{r^2}\right)-\frac{\sigma}{2}\left(1+\frac{3R^4}{r^4}\right)\cos 2\theta \tag{A2}$$

$$\sigma_{r\theta} = -\frac{\sigma}{2}\left(1-\frac{3R^4}{r^4}+\frac{2R^2}{r^2}\right)\sin 2\theta \tag{A3}$$

where the Cartesian xy, and polar rθ coordinate systems are introduced in Fig. A1b. It should be emphasized that the planar Kirsch problem describes the plane-stress case, i.e.

$$\sigma_{zz} = 0 \tag{A4}$$

where z is the third Cartesian coordinate normal to x and y and should not cause any confusion with the complex variable z=y+ix (with i being the imaginary unity introduced in Fig. A1b). It should be emphasized that the non-standard introduction of the complex

variable z is related to the fact that in Fig. A1b the angle θ is reckoned from the axis of stretching y, rather than from the x-axis. Still, $z=re^{i\theta}$.

The corresponding Airy function U, which is the solution of the biharmonic equation $\nabla^4 U = 0$ of the planar theory of elasticity, can be found from Eqs. (A1)-(A3) using the following relations [32]

$$\sigma_{rr} = \frac{1}{r}\frac{\partial U}{\partial r} + \frac{1}{r^2}\frac{\partial^2 U}{\partial \theta^2}, \quad \sigma_{\theta\theta} = \frac{\partial^2 U}{\partial r^2}, \quad \sigma_{r\theta} = -\frac{\partial}{\partial r}\left(\frac{1}{r}\frac{\partial U}{\partial \theta}\right) \tag{A5}$$

It reads

$$U = \frac{\sigma}{2}\left(\frac{r^2}{2} - R^2 \ln r\right) - \frac{\sigma}{4}\left(r^2 + \frac{R^4}{r^2} - 2R^2\right)\cos 2\theta \tag{A6}$$

The Airy function U is determined by the two Goursat functions (or the complex elastic potentials) φ(z) and χ(z) as [26]

$$U = \mathrm{Re}\left\{\bar{z}\varphi + \chi\right\} \tag{A7}$$

Comparing Eqs. (A6) and (A7), it is easy to see that

$$\varphi(z) = \frac{\sigma z}{4} + \frac{\sigma}{2}\frac{R^2}{z}, \quad \chi(z) = -\frac{\sigma R^2}{2}\ln z - \frac{\sigma}{4}\left(z^2 + \frac{R^4}{z^2}\right) \tag{A8}$$

It is convenient to introduce a new function $\psi(z) = \chi'(z)$, i.e.

$$\psi(z) = -\frac{\sigma R^2}{2z} - \frac{\sigma}{2}\left(z - \frac{R^4}{z^3}\right) \tag{A9}$$

which will be used below.

It should be emphasized that the same functions φ(z) and $\psi(z)$ can be found using Eqs. (A1)-(A3) and the stresses

$$\sigma_{xx} = \sigma_{rr}\sin^2\theta + \sigma_{r\theta}\sin 2\theta + \sigma_{\theta\theta}\cos^2\theta \tag{A10}$$

$$\sigma_{xy} = \left(\sigma_{rr} - \sigma_{\theta\theta}\right)\frac{1}{2}\sin 2\theta + \sigma_{r\theta}\cos 2\theta \tag{A11}$$

$$\sigma_{yy} = \sigma_{rr}\cos^2\theta - \sigma_{r\theta}\sin 2\theta + \sigma_{\theta\theta}\sin^2\theta \tag{A12}$$

having in mind that

$$\sigma_{xx} + \sigma_{yy} = 4\,\mathrm{Re}\{\varphi'\} \tag{A13}$$

$$\sigma_{xx} - \sigma_{yy} + 2i\sigma_{xy} = \left(\bar{z}\varphi'' + \psi'\right) \tag{A14}$$

Accordingly, the displacements along the y and x axes, v and u, respectively, are found as [26]

$$v + iu = \frac{1}{2G}\left[\kappa\varphi - z\overline{\varphi'(z)} - \overline{\psi(z)}\right] \tag{A15}$$

where the shear modulus G is given by

$$G = \frac{E}{2(1+\nu)} \tag{A16}$$

with E being Young's modulus and ν is Poisson's ratio. Also,

$$\kappa = \frac{3-\nu}{1+\nu} \tag{A17}$$

for the plane stress problem (A4) [33].

Solution of the problem with a circular elastic inclusion can be constructed as a linear superposition of three problems (Fig. A2). Problem (I) is a uniform biaxial stretching with the dimensionless factors k_x and k_y to be found, and problems (II) and (III) being the Kirsch problems. Such a linear superposition is possible due to linearity of the theory of elasticity and the fact that the boundary conditions for stretching at infinity for the uniaxial stretching are satisfied by it. Moreover, it will be shown below that the boundary condition at the interface of the inner material 2 and the outer material 1, which

is the requirement that the displacements are identical on both banks of the interface (since the materials are bonded), can also be satisfied by the choice of the factors k_x and k_y.

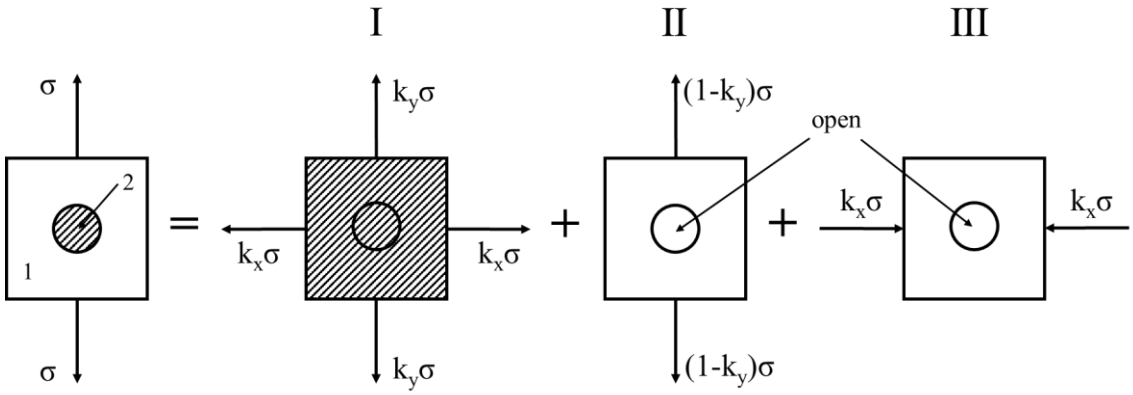

Fig. A2. Split of the problem on stretching of elastic material (1) with a circular elastic inclusion (2) into a linear superposition of three problems (I), (II) and (III).

The uniform biaxial stretching in the inner material 2, as well as in the outer material for problem I is given by the following elastic potentials

$$\varphi(z)=\frac{(k_x+k_y)\sigma}{4}z,\quad \psi(z)=\frac{(k_x-k_y)\sigma}{4}z \tag{A18}$$

Using Eqs. (A8), (A9), (A15) and (A18), and superimposing the solutions for problems I, II, and III, one can find the displacement field in the outer material in the case of uniaxial stretching along the y-axis of an elastic material 1 with a circular elastic inclusion in the following form

$$v=\frac{\sigma}{E_1}\left(k_y-\nu_1 k_x\right)y+\frac{\left(1-k_y\right)\sigma}{2G_1}\mathrm{Re}\left\{\kappa_1\left(\frac{z}{4}+\frac{R^2}{2z}\right)-z\left(\frac{1}{4}-\frac{R^2}{2\bar{z}^2}\right)+\frac{R^2}{2\bar{z}}+\frac{1}{2}\left(\bar{z}-\frac{R^4}{\bar{z}^3}\right)\right\}$$
$$-\frac{k_x\sigma}{2G_1}\mathrm{Im}\left\{\kappa_1\left(\frac{z_1}{4}+\frac{R^2}{2z_1}\right)-z_1\left(\frac{1}{4}-\frac{R^2}{2\bar{z}_1^2}\right)+\frac{R^2}{2\bar{z}_1}+\frac{1}{2}\left(\bar{z}_1-\frac{R^4}{\bar{z}_1^3}\right)\right\} \tag{A19}$$

$$u=\frac{\sigma}{E_1}\left(k_x-\nu_1 k_y\right)x+\frac{\left(1-k_y\right)\sigma}{2G_1}\mathrm{Im}\left\{\kappa_1\left(\frac{z}{4}+\frac{R^2}{2z}\right)-z\left(\frac{1}{4}-\frac{R^2}{2\bar{z}^2}\right)+\frac{R^2}{2\bar{z}}+\frac{1}{2}\left(\bar{z}-\frac{R^4}{\bar{z}^3}\right)\right\}$$
$$-\frac{k_x\sigma}{2G_1}\mathrm{Re}\left\{\kappa_1\left(\frac{z_1}{4}+\frac{R^2}{2z_1}\right)-z_1\left(\frac{1}{4}-\frac{R^2}{2\bar{z}_1^2}\right)+\frac{R^2}{2\bar{z}_1}+\frac{1}{2}\left(\bar{z}_1-\frac{R^4}{\bar{z}_1^3}\right)\right\} \tag{A20}$$

where subscript 1 corresponds to material 1 and

$$z=y+ix,\quad z_1=x-iy \tag{A21}$$

In the inner material 2, accordingly,

$$v=\frac{\sigma}{E_2}\left(k_y-\nu_2 k_x\right)y \tag{A22}$$

$$u=\frac{\sigma}{E_2}\left(k_x-\nu_2 k_y\right)x \tag{A23}$$

With $y=R\cos\theta$ and $x=R\sin\theta$, i.e. at the interface, Eqs. (A19)-(A21) yield

$$v=\frac{\sigma}{E_1}\left(k_y-\nu_1 k_x\right)y+\frac{3\left(1-k_y\right)\sigma}{E_1}y+\frac{k_x\sigma}{E_1}y \tag{A24}$$

$$u=\frac{\sigma}{E_1}\left(k_x-\nu_1 k_y\right)x-\frac{\left(1-k_y\right)\sigma}{E_1}x-\frac{3k_x\sigma}{E_1}x \tag{A25}$$

Equating Eqs. (A22) and (A23) with Eqs. (A24) and (A25), respectively, to satisfy the condition of the identical displacements of both materials at the interface (the bonding condition), one obtains a system of two equations for two unknowns, k_x and k_y, which yields

$$k_x = \frac{E_2\left[E_1\left(-1+3\nu_2\right)+E_2\left(1-3\nu_1\right)\right]}{\left(E_1+2E_2\right)^2-\left[\nu_2 E_1+E_2\left(1-\nu_1\right)\right]^2} \tag{A26}$$

$$k_y = \frac{E_2\left[\left(3-\nu_2\right)E_1+E_2\left(5+\nu_1\right)\right]}{\left(E_1+2E_2\right)^2-\left[\nu_2 E_1+E_2\left(1-\nu_1\right)\right]^2} \tag{A27}$$

In the case of very stiff inclusions when the ratio $E_2 / E_1 \to \infty$, Eqs. (A26) and (A27) are reduced to the following ones

$$k_x = \frac{1-3\nu_1}{3+2\nu_1-\nu_1^2}, \quad k_y = \frac{5+\nu_1}{3+2\nu_1-\nu_1^2} \tag{A28}$$

Then, the displacements in material 1 along the stretching axis y, i.e. at x=0, are found from Eqs. (A19)-(A21) as

$$\begin{aligned} v\big|_{x=0} = {} & \frac{\sigma}{E_1}\left(k_y-\nu_1 k_x\right)y+\frac{\left(1-k_y\right)\sigma}{2G_1}\left[\kappa_1\left(\frac{y}{4}+\frac{1}{2y}\right)-y\left(\frac{1}{4}-\frac{1}{2y^2}\right)+\frac{1}{2y}+\frac{1}{2}\left(y-\frac{1}{y^3}\right)\right] \\ & -\frac{k_x\sigma}{2G_1}\left[\kappa_1\left(-\frac{y}{4}+\frac{1}{2y}\right)+y\left(\frac{1}{4}+\frac{1}{2y^2}\right)-\frac{1}{2y}+\frac{1}{2}\left(y-\frac{1}{y^3}\right)\right] \end{aligned} \tag{A29}$$

$$u\big|_{x=0} = 0 \tag{A30}$$

The stress fields in the outer material 1 can be found as a superposition of the corresponding stress fields for problems I and II and II. Namely, for the combination of problems I and II, we obtain from Eqs. (A8), (A9), (A13) and (A14)

$$\sigma_{xx} = \mathrm{Re}\left\{\bar{z}\varphi''+\psi'+2\varphi'\right\} \tag{A31}$$

$$\sigma_{yy} = -\mathrm{Re}\left\{\bar{z}\varphi''+\psi'-2\varphi'\right\} \tag{A32}$$

$$\sigma_{xy} = \mathrm{Im}\left\{\bar{z}\varphi''+\psi'\right\} \tag{A33}$$

where primes denote derivatives by z, and

$$\varphi' = \frac{\left(k_x + k_y\right)\sigma}{4} + \frac{\left(1-k_y\right)\sigma}{4} - \frac{\left(1-k_y\right)\sigma}{2}\frac{R^2}{z^2}, \quad \varphi'' = \left(1-k_y\right)\sigma\frac{R^2}{z^3} \tag{A34}$$

$$\psi' = \frac{\left(k_x - k_y\right)\sigma}{2} + \frac{\left(1-k_y\right)\sigma R^2}{2z^2} - \frac{\left(1-k_y\right)\sigma}{2}\left(1+\frac{3R^4}{z^4}\right) \tag{A35}$$

Accordingly, the stress field corresponding to problem III reads

$$\sigma_{xx} = -\mathrm{Re}\left\{\bar{z}_1\varphi'' + \psi' - 2\varphi'\right\} \tag{A36}$$

$$\sigma_{yy} = \mathrm{Re}\left\{\bar{z}_1\varphi'' + \psi' + 2\varphi'\right\} \tag{A37}$$

$$\sigma_{xy} = \mathrm{Im}\left\{\bar{z}_1\varphi'' + \psi'\right\} \tag{A38}$$

where primes denote derivatives by z_1, and

$$\varphi' = \frac{k_x\sigma}{4} + \frac{k_x\sigma}{2}\frac{R^2}{z_1^2}, \quad \varphi'' = -k_x\sigma\frac{R^2}{z_1^3} \tag{A39}$$

$$\psi' = -\frac{k_x\sigma R^2}{2z_1^2} + \frac{k_x\sigma}{2}\left(1+\frac{3R^4}{z_1^4}\right) \tag{A40}$$

Adding Eq. (A31) to (A36), Eq. (A32) to (A37) and Eq. (A33) to (A38), one obtains all the fields of the stress components in the outer material 1.

In inner material 2, Eqs. (A18) yield

$$\varphi' = \frac{\left(k_x + k_y\right)\sigma}{4}, \quad \varphi'' = 0, \quad \psi' = \frac{\left(k_x - k_y\right)\sigma}{2} \tag{A41}$$

which with Eqs. (A30)-(A32)] yield the stress fields in these materials.

References

[1] Michielsen S, Pourdeyhimi B, Desai P. Journal of Applied Polymer Science 2006; 99: 2489–2496.

[2] Brown HR, J. Res. and Develop 1994; 38: 379-389.

[3] Clarke CJ, Polymer 1996; 37: 4747-4752.

[4] Geoghegan M, Clarke CJ, Boue F, Menelle A, Russ T, Bucknall DG, Macromolecules 1999; 32: 5106-5114.

[5] Jenkins ML, Dauskardy RH, Bravman JC, Journal of Adhesion Science and Technology 2004; 18:1497-1516.

[6] Baldan A, International Journal of Adhesion & Adhesives 2012; 38: 95-116.

[7] Islam A, Hansen HN, Bondo M, Int J Adv Manuf Technol 2010; 50: 101-111.

[8] O'Connor KP, McLeish TCB, Faraday Discuss 1994; 98: 67-78.

[9] O'Connor KP, McLeish TCB, Macromolecules 1993; 26: 7322-7325.

[10] Bhat, GS, Jangala, PK, Spruiell, JE. (2004). Journal of Applied Polymer Science 2004; 92: 3593-3600.

[11] Dangseeyun, N, Supaphol, P, Nithitanakul. M. Polymer testing 2004; 23: 187-194.

[12] Keller, A, Lester, GR, Morgan, LB. Phil. Trans. R. Soc. Lond. A 1954; 247:1-12.

[13] Stein, RS, Misra, A. Journal of Polymer Science Part B: Polymer Physics 1980; 18:327-342.

[14] Lin, W, Cossar, M, Dang, V,Teh, J. Polymer testing 2007; 26: 814-821.

[15] Hughes, CD, Sethi, NK, Baltisberger, JH, Grant, DM. Macromolecules 1989; 22: 2551-2554.

[16] Aggarwal, SL, Tilley, GP. Journal of Polymer Science Part A: Polymer Chemistry 1955; 18: 17-26.

[17] Hegde, RR, Bhat, GS, Campbell, RA. Journal of applied polymer science 2008; 110: 3047-3058.

[18] Wang X, Michielsen S, Textile Research Jounral 2002; 72: 394-398.

[19] Fedorova N, Verenich S, Pourdeyhimi B, Journal of Engineered Fibers and Fabrics 2007; 2: 38-48.

[20] Wang X, Michielsen S, Textile Research Jounral 2001; 71: 475-480.

[21] Dasdemir M, Maze B, Anantharamaiah N, Pourdeyhimi B, Journal of Material Science 2012; 47: 5955-5969

[22] Kirsch G. Zantralblatt Verlin Deutscher Ingenieure 1898; 43: 797-807.

[23] Eshelby DE. Proc. Roy. Soc. London A 1957; 241: 376-396.

[24] Eshelby DE, Proc. Roy. Soc. London A 1959; 252: 561-569.

[25] Deryugin YY, Lasko GV, Engineering 2012; 4: 583-589.

[26] Muskhelishvili NI, *Some Basic Problems of the Mathematical Theory of Elasticity,* Noordhoff International Publishing, Leyden 1975.

[27] England AH, *Complex Variable Methods in Elasticity,* John Wiley & Sons, New York 1971.

[28] Galin LA, *Contact Problems,* Springer, Heidelberg 2008.

[29] Mandal BK, *Polymer Synthesis-Strategies and Tactics,* Covalent Press, Inc. 2009.

[30] Green AE, Proc. Roy. Soc. London A 1956; 234: 46-59.

[31] Yarin AL, Pourdeyhimi B, Ramakrishna S, *Fundamentals and Applications of Micro and Nanofibers,* Cambridge University Press, Cambridge 2014.

[32] Landau LD, Lifshitz EM, *Theory of Elasticity,* 2nd ed., Pergamon Press, Oxford 1970.

[33] Cherepanov GP, *Mechanics of Brittle Fracture,* McGraw Hill, New York 1979.